Journal Pre-proof

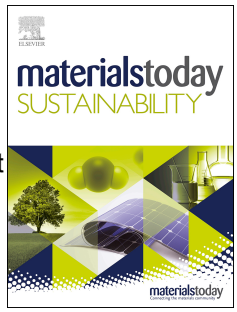

A novel hybrid enhanced oil recovery technique to enhance oil production from oil-wet carbonate reservoirs by combining electrical heating with nanofluid flooding

Farida Amrouche, Martin J. Blunt, Stefan Iglauer, Farid Aiouache, Michael Short

PII: S2589-2347(24)00251-3

DOI: https://doi.org/10.1016/j.mtsust.2024.100915

Reference: MTSUST 100915

To appear in: *Materials Today Sustainability*

Received Date: 1 April 2024

Revised Date: 13 June 2024

Accepted Date: 8 July 2024

Please cite this article as: F. Amrouche, M.J. Blunt, S. Iglauer, F. Aiouache, M. Short, A novel hybrid enhanced oil recovery technique to enhance oil production from oil-wet carbonate reservoirs by combining electrical heating with nanofluid flooding, *Materials Today Sustainability*, https://doi.org/10.1016/j.mtsust.2024.100915.

A novel hybrid enhanced oil recovery technique to enhance oil production from oil-wet carbonate reservoirs by combining electrical heating with nanofluid flooding

Farida Amrouche[1], Martin J. Blunt[2], Stefan Iglauer[3], Farid Aiouache[1], Michael Short[4]

[1]School of Engineering, Lancaster University, Lancaster LA1 4YW, United Kingdom

[2]Department of Earth Science and Engineering, Imperial College London, Exhibition Road, London SW7 2AZ, United Kingdom

[3]School of Engineering, Edith Cowan University, 270 Joondalup, WA 6027, Australia

[4]School of Computing, Engineering & Digital Technologies, Teesside University, Middlesbrough TS1 3BX, United Kingdom

Abstract

Enhanced Oil Recovery provides a promising technique to maximise fossil fuel recovery from existing resources, and when used in conjunction with Carbon Capture and Storage/Utilisation provides a way to support a transition to alternative cleaner fuels. A hybrid Enhanced Oil Recovery method by a combination of electrical heating and nanofluid flooding was applied to oil-wet carbonate reservoirs and assessed in terms of the oil production, zeta potential, contact angle, pellet compaction, interfacial tension, and pH values. The hybrid technique consisted of a combination of direct current (up to 30 V) and iron oxide (Fe_2O_3) or magnesium oxide (MgO) nanofluids. Both nanofluids were injected into oil-wet Austin chalk – our laboratory model of an oil-wet carbonate reservoir – and then electrical heating was started, or vice versa. Introducing electrical heating first increased oil recovery by up to 27% in seawater compared to 16% in deionised water. When Fe_2O_3 nanofluid was injected, oil recovery further increased to 32% in seawater and 24% in deionised water. The contact angle and zeta potential decreased from 124^o to 36^o and from -24.4 to -23.7 mV, respectively, when nanofluid was injected in seawater, leading to better nanofluid stability and penetration into the carbonate rock as shown by increased pellet porosity from 6.6% to 14.8%. Moreover, it was found that the interfacial tension was reduced from 72 to 32.7 mN/m in the pre-magnetised samples with Fe_2O_3 NPs injection compared to

33.2 mN/m in the samples with MgO injection. It was found from our experiments that the effect of the generated electricity on the surface charge was of a temporary nature as the zeta potential of the rock returned to its original value as soon as the power was disconnected. The mechanism underlying the hybrid Enhanced Oil Recovery EOR technique from the laboratory findings was found to be based on electrowetting and nanofluid adsorption. Results indicate that the technique is promising for further improving oil recovery and securing energy supply during the transition to net zero.

Keywords: EOR; Electrical heating; Nanoparticles; Zeta potential; Wettability; Carbonate rock; Energy transition.

Nomenclature

API	American Petroleum Institute
CCS	Carbon Capture and Storage
DC	Direct Current
ddH_2O	Double Distilled Water
DSA	Drop Shape Analyser
DW	Deionised Water
EOR	Enhanced Oil Recovery
EH	Electrical Heating
EM	Electromagnetic
FB	Formation brine
Kw	Absolute Permeability to Water
Mag	Magnets
md	Millidarcy
MF	Magnetic Field
NPs	Nanoparticles
PDIs	Potential Determining Ions
ppm	Parts Per Million
RF	Recovery Factor
SEM	Scanning Electron Microscope

SW	Seawater
Swi	Initial Water Saturation
V	Voltage
Wf	Wedge Film
wt%	Weight Percentage
Al_2O_3	Alumina
$CaCl_2.2H_2O$	Calcium Chloride
Fe_2O_3	Iron Oxide
KCl	Potassium Chloride
($MgCl_2.H_2O$)	Magnesium Chloride
MgO	Magnesium Oxide
$NaHCO_3$	Sodium Bicarbonate
NaCl	Sodium Chloride
Na_2SO_4	Sodium Sulphate
S/cm	Siemens Per Centimetre
SO_4^{2-}	Sulphate
ZnO-NCs	Zinc Oxide Nanocrystals
Δt	Time
$\Delta\Upsilon$	Disjoining Pressure

1. Introduction

Environmental issues, coupled with the depletion of finite resources and economic concerns, have motivated governments worldwide to take pressing action to reduce reliance on fossil fuels and promote the transition towards a net zero emissions society [1]. Although advances have been achieved in renewable energy technology, there remains much work to be done. Careful management of the transition to net zero carbon needs to address continuing fossil fuel production [1,2]. In this context, there has been interest in Enhanced Oil Recovery (EOR) techniques to maximise fossil fuel recovery from existing natural resources, which could be integrated with Carbon Capture and Storage (CCS) techniques to reduce atmospheric emissions [3].

EOR techniques continue to gain attention because conventional primary and secondary oil recovery methods reach recoveries of 30-50% of the crude oil in place [4,5]. Heavy oil, which accounts for 70% of total world oil reserves [6] is a particular target for innovative EOR technologies. Electrical heating (EH) is a technology for recovering heavy oil whereby heat is used to warm up the reservoir fluids without losing much heat to the environment [7,8]. EH was introduced as an eco-friendly technique since it reduces water use in both shale and conventional reservoir environments [9]. In addition, there is a growing interest in introducing hybrid techniques to boost oil production by using nanoparticles (NPs) associated with EH and magnetic fields (MFs). For example, it has been found that adding an MF before the introduction of NPs improves ultimate oil recovery because the solution becomes pre-magnetised [10] while the addition of an MF (4,500 G) to 0.8 wt% ferrofluid NPs during water flooding increased the oil recovery factor (RF%) by 10% [11].

In previous work, forty-times diluted nanofluid in seawater resulted in 41% lower interfacial tension and a 40% decrease in contact angle with carbonate rock samples, indicating a transition to more water-wet conditions, which eventually enhanced final oil recovery for secondary and tertiary EOR by 13.7% and 8.3%, respectively [12]. The magnesium (Mg^{2+}) and calcium (Ca^{2+}) divalent ions present in the injected saline water were critical because they were adsorbed to the solid matrix [13]. A new approach has been adopted in recent studies to increase oil recovery through the combination of an electric field with nanofluids in the reservoir. It was found that the introduction of an electric field with nanofluids helps lower the oil/water interfacial tension a lot more effectively than nanofluids alone [14]. The preferred distribution of particles at the fluid/oil interface reduced interfacial tension between the fluid and oil when nanosized particles are added to the injection fluids [15]. Smaller nanoparticles improved wettability (made the samples more water-wet) by increasing the electrostatic repelling force and disjoining pressure. Smaller nanoparticles could easily pass through the narrow pore throats of the rock, preventing entrapment [16]. Metal oxides, silica, and polymers are the three most prevalent nanoparticle kinds employed in EOR. Metal oxides, such as iron oxide, and aluminium oxide help release trapped oil and lower interfacial tension [17]. However, few systematic experimental studies have been performed to ascertain the effectiveness of this EOR technique and the possible mechanisms by which

it works. Using 0.05 wt% Fe_2O_3 NPs in the presence of electromagnetic (EM) waves during water injection into a sandstone resulted in a 6.1% decrease in interfacial tension, and a 13.6% increase in ultimate oil recovery [18]. Nanomaterials (or nanofluids) can be used in conjunction with electrical heating to improve heavy oil extraction because they alter rock wettability, reduce fluid viscosity, increase thermal conductivity, and change interfacial tension, thereby altering the molecular interaction between the various interfaces [14]. Most of the previous research used electromagnetic fields combined with nanoparticles. For instance, the self-assembling of zinc oxide nanocrystals (ZnO-NCs) resulted in an increase in the local viscosity of the nanofluid at the water-oil interface, which in turn resulted in a 50% increase in recovery efficiency compared to displacement without EM energy. This study demonstrated the ability of EM energy to increase the viscosity of the injected ZnO-NF in the porous medium, resulting in a 23.3% increase in recovery efficiency via the electrorheological effect of the activated dielectric ZnO-NCs. The later caused a change in the rheological properties (e.g. viscosity, stress, and shear modulus), indicating that the suspended nanoparticles were polarised under the applied electrical field and instantly restored their initial state when the field was disconnected [19].

EH tests were conducted in glass bead packs filled with crude oil in the presence of 0.1-1wt% Fe_2O_3, copper or nickel NPs, resulting in a viscosity reduction of 10-20% [20]. It has been proposed that by placing NPs in an electrical field, water production could be reduced by blocking pore throats via the electrorheological effect [21]. Due to the electrorheological properties of a dielectric nanofluid made from alumina (Al_2O_3), the injection of NPs into a silica bead pack increased oil recovery to 54.2% [22]. However, there have been only a few experimental trials using Fe_2O_3 NPs combined with an EH [23]. It is noteworthy to mention that the existing research in this area has been limited because, across the various studies described, sandstone or glass beads were used more than any other material, so more research needs to be carried out on carbonates (which contain most conventional hydrocarbons). Existing studies also suggest a lack of understanding of the underlying mechanisms [24,25].

This work introduces a hybrid experimental technique for oil-wet carbonate reservoirs that combines EH with Fe_2O_3 and MgO NPs, which were both separately dispersed in deionised water (DW) and

99 seawater (SW), helping to improve oil recovery at reduced use of chemicals and DC current. This
100 technique is novel by introducing EH generated by a DC current and through the assessment
101 of several physiochemical parameters (i.e. contact angle, zeta potential and interfacial tension).
102 Also, the results were interpreted in the context of the propagation of a wedge film associated
103 with wettability alteration. Finally, the mechanisms leading to improved recovery and large-
104 scale design related to EH with nanoparticles are postulated from the laboratory findings.

105 **2. Materials and Methods**

106 **2.1 Materials**

107 The model rock was Austin chalk (permeability: 8-15 md, porosity: 25-27%), while the model oil used
108 was a 0.01 M stearic acid solution in *n*-decane (density = 0.730 kg/m^3 at 20^{o}C, and viscosity 0.69 mPa.s)
109 [3]. Austin chalk composition, materials purities and suppliers, and seawater (SW) composition are
110 given in **Tables 1** to **3**.

Table 1. Elemental composition (in atom%) of Austin chalk (measured via energy dispersive X-ray spectroscopy).

C	O	Mg	Al	Si	Ca	Fe
10.08	45.06	0.2	0.09	0.28	44.03	0.26

111

Table 2. Material purities and suppliers.

Material	Purity	Diameter	Supplier
Austin chalk core		25 mm	Kocurek Industries, Texas, USA
Iron oxide (Fe_2O_3)	99mol%	<50 nm	Aldrich
Magnesium oxide (MgO)	99mol%	<50 nm	Aldrich
n-decane	99%		Merck
Stearic acid	≥90%		Alfa Aesar
Toluene	99%		Fisher Chemicals
2-Propanol	99%		VWR Chemicals UK

112

Table 3. Seawater (SW) composition.

Salt	*Sodium Chloride (NaCl)*	*Sodium Sulphate (Na_2SO_4)*	*Potassium Chloride (KCl)*	*Sodium Bicarbonate ($NaHCO_3$)*	*Magnesium Chloride ($MgCl_2{\cdot}6H_2O$)*	*Calcium Chloride ($CaCl_2{\cdot}2H_2O$)*
Mass (g/L)	23.926	4.008	0.677	0.196	10.831	1.5199

2.2 Methods

2.2.1 Core preparation

Austin chalk cores were completely soaked in toluene for 48 hours to remove impurities and dried in a desiccator for 24 hours at 70°C. Subsequently, the diameter, length, and dry weight of the cores were measured. Then the samples were introduced into a vacuum saturator until they were saturated with 100% deionised water (DW). Note that the cores imbibed DW immediately once the vacuum was lifted, hence, a pressure of 3.44×10^6 Pa was introduced to the sample for 3 hours to push DW inside the cores and ensure that no air was left in the pore space. After this, the pressure was released, and the cores were left for 8-10 hours to ensure that they were completely saturated. Before placing the cores in a Vinci core holder, the wet weight was measured to determine the pore volume and porosity, 5-6 PV of DW and model oil (0.01 m stearic acid mixed in n-decane) were injected, and the absolute permeability to water and initial water saturation (S_{wi}) were measured (the capillary number during oil injection was 2.4×10^{-5}). Next, the cores were immersed in the model oil and left for 30 days at 40°C (at constant lab pressure). This is a process called ageing during which the wettability of the rock is rendered more oil-wet due to stearic acid adsorption on the chalk surface, see **Fig. 1** [10]. The sample properties are given in **Table 4**.

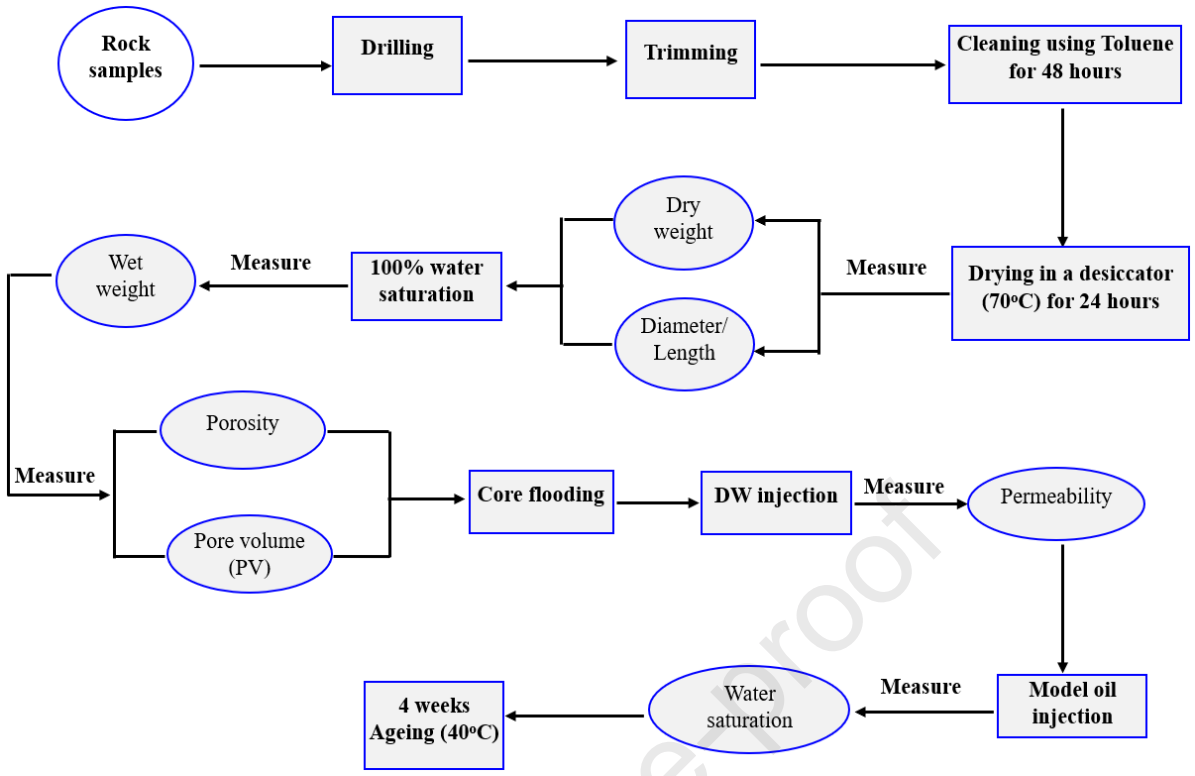

Fig. 1. Core preparation methodology used for this study.

Table 4. Chalk core properties.

	Diameter (mm)	Length (mm)	Dry weight (g)	Pore volume (PV) (ml)	Porosity (%)	Absolute Perm water (K_w) (mD)	Initial water saturation (S_{wi})
Core #1 Fe_2O_3 mixed in DW added before EH	25.1	69.9	67.7	9.7	28.1	11.6	19.8
Core #2 Fe_2O_3 mixed in SW added before EH	25.0	69.9	66.0	9.8	28.7	15.0	26.8
Core #3 Fe_2O_3 mixed in DW added after EH	25.0	69.9	65.7	9.7	28.2	15.0	24.6
Core #4 Fe_2O_3 mixed in SW added after EH	25.1	69.7	65.5	9.8	28.5	15.0	27.8
Core #5 MgO mixed in DW added before EH	25.0	69.8	65.8	9.9	28.9	9.7	28.0
Core #6 MgO mixed in SW added before EH	25.0	69.9	67.6	9.7	28.3	12.8	27.1
Core #7 MgO mixed in DW added after EH	25.0	69.8	66.0	9.9	15.6	15.0	29.9

Core #8 MgO mixed in SW added after EH	25.0	69.7	65.1	9.9	29.9	14.7	26.8

2.2.2 Nanofluid preparation

Nanofluid was formulated by adding a specified concentration of NPs (in wt%) to 1L of deionised water (DW) of conductivity 1 S/cm or seawater (SW) of conductivity 540 S/m, and 28,000 ppm salinity, respectively. The resultant mixture was stirred for 40 minutes before being heated for 15 minutes on a hot plate at 70^{o}C. Then, 20 mL of 2-propanol were added to the mixture. After that, the nanofluid was placed in a sonic bath for two hours to improve the suspension and avoid agglomeration. The dispersion was allowed to cool to room temperature before being introduced to the sample [10].

2.2.3 Spontaneous imbibition experiments

After 30 days of ageing, the cores were placed inside Amott cells and immersed in DW/NP nanofluids, in the presence or absence of EH of 15-30 V. A direct current (DC) of up to 30 V was applied to the Amott cells during spontaneous imbibition, using a cable with 2,160 turns of 0.8 mm diameter, 625 m in length, and 30 Ω total resistance (provided by RS PRO UK) added around a metal cup slightly larger in diameter than the Amott cells [3]. The Amott cell was not wrapped directly with the electrical coil. However, it was placed inside a metallic cup and an electrical coil was added. There was a combined effect of heat of ~ 40^{o}C and an induced magnetic field up to 20 mT [3]. The magnetic field was too small to have a significant effect on its own, only by combining it with the generated heating did oil production increase. Hence, the physical process was named electrical heating. **Fig. 2** and **Fig. 3** present the experimental apparatus and a summary of the experimental procedure used during spontaneous imbibition, respectively.

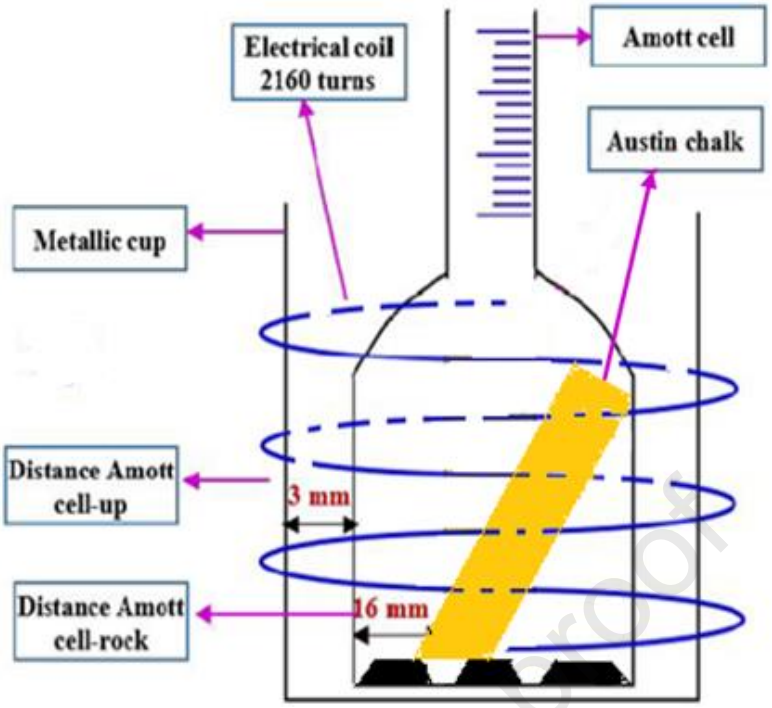

155

156 **Fig. 2.** The experimental apparatus used to study spontaneous imbibition apparatus using electrical heating.

157

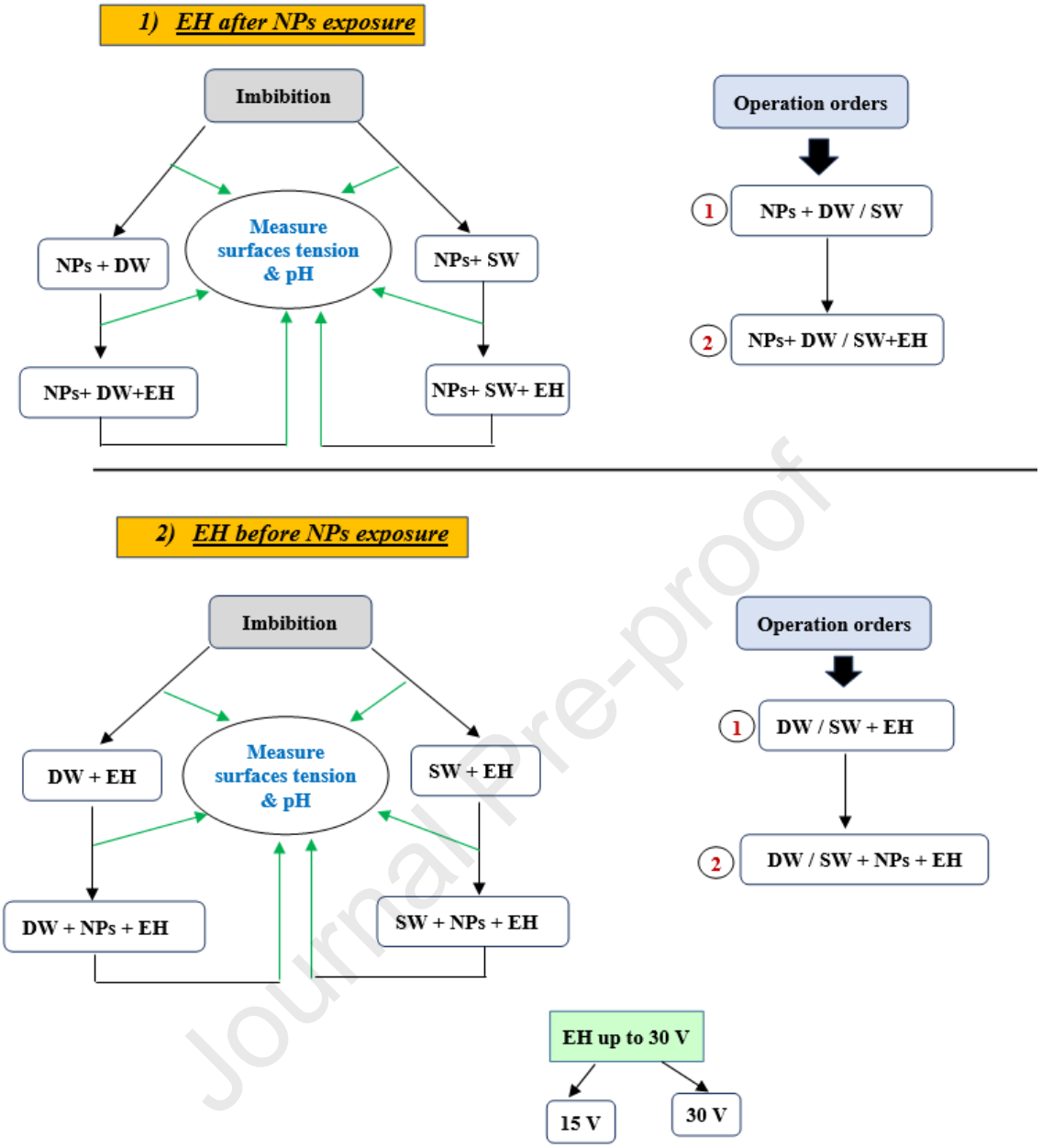

Fig. 3. Laboratory flowchart for the spontaneous imbibition experiments.

2.2.4 pH and interfacial tension measurements

At room temperature, the pH and interfacial tension between the imbibing fluid and air with and without EH (before, and at the end of spontaneous imbibition of each stage of the process) were measured using a K9 Kruss GMBH tensiometer and Hanna pH probe (**Fig. 3**).

2.2.5 Contact angle measurements

To characterise the wettability by contact angle measurements, a core sample was pressed into pellets. Specifically, 1g of dried, crushed, and sieved core was subjected to a force of 9 tonnes via a SPECAC (England) press, to ensure that the pellets were uniform in size and shape and texture, and to thus avoid irregularities in contact angle measurements that would occur if the surface was uneven (note that the pellets were flat). A DSA 100 goniometer (Germany) was used to measure the contact angle in real-time (until reaching pellet saturation and no further decrease in the contact angle was observed); thus, double distilled water (ddH_2O with a conductivity of 0.05 µS/cm) drops were dispensed on the pellets (3 measurements carried out on each pellet $\pm$0.2%). SEM images were also acquired for some of the prepared pellets, and the porosity of the pellets was measured on the SEM images with Dewinter Material Plus software [10]. In addition, after 30 days of spontaneous imbibition, the cores were dried, crushed, and sieved to 400-560 µm using an American Petroleum Institute (API) sieve, and the contact angles on the fragments were measured.

2.2.6 Zeta potential measurements

As mentioned above, after 30 days of spontaneous imbibition, the cores were dried, crushed, and sieved to 400-560 µm using an API sieve, and the zeta potential of the fragments was measured. Two scenarios were investigated: firstly, a DC up to 9 V around the measuring cell was applied around a packing of crushed and sieved powder of the aged core to measure the surface charge (**Fig. S1**). The characteristics of the generated MF are tabulated in **Table S1**.

Secondly, zeta potentials were measured without introducing an EH at the end of each spontaneous imbibition experiment, using an electrokinetic analyser (Anton Paar, UK), as described previously.

3. Results and discussion

The effect of a combination of NP (here Fe_2O_3 NPs) and EH as a hybrid technique on contact angle, zeta potential and porosity of the core samples was evaluated (see **Table 5**); and the difference between

DW and SW systems (in terms of oil recovery, interfacial tension, and pH) during spontaneous imbibition was assessed. We see from Table 5 that SW gives lower contact angles than DW, indicating more water-wet conditions. This could be due to the salinity itself, or the better dispersion of nanoparticles in SW.

3.1. Impact of Fe_2O_3/MgO NPs exposed to EH on contact angle and zeta potential

The results from the contact angle, zeta potential and pellet`s porosity are displayed in **Table 5**.

Table 5. Contact angle and zeta potential of cores before and after imbibition.

	Contact angle (º)	**Zeta potential (mV)**	**Pellet Porosity (%)**
Modified core (oil-wet without imbibition)	124	-24.4	6.6
DW OW reference core (no EH)	105	-22.2	7.9
DW OW+EH	84	-16.6	9.2
SW OW reference core (no EH)	89	-25.8	11.3
SW OW+ EH	62	-26.9	12.7
Core #1 Fe_2O_3 mixed in DW added before EH	35	-19.9	13.4
Core #2 Fe_2O_3 mixed in SW added before EH	31	-18.6	13.8
Core #3 Fe_2O_3 mixed in DW added after EH	39	-23.5	14.6
Core #4 Fe_2O_3 mixed in SW added after EH	36	-23.7	14.8
Core #5 MgO mixed in DW added before EH	69	-25.5	11.8
Core #6 MgO mixed in SW added before EH	65	-28.3	13.1
Core #7 MgO mixed in DW added after EH	54	-27.5	12.1
Core #8 MgO mixed in SW added after EH	52	-32.9	13.2

The effect of EH on contact angle allowing for the faster onset of imbibition was demonstrated by Amrouche et al., (2022). For instance, the time to reach a 90^o contact angle took 52 min for samples without the effect of EH to 17 min for samples subjected to 9 V. The contact angle and zeta potential of the modified (oil-wet without imbibition) core were 123.8^o and -24.4 mV, respectively [26,27]. When

Fe_2O_3 NPs mixed in DW were introduced into **core #1** and **core #2** before and after EH, the contact angle decreased from 123.8° to 35° and 31°, respectively. Furthermore, the zeta potential was reduced from -24.4 mV to -19.9 mV in **core #1**, and to -18.6 mV in **core #2**. Similarly, when Fe_2O_3 NPs were mixed in SW, the contact angle decreased to 39° in **core #3** and 36° in **core #4**. In addition, EH pre-heated and pre-magnetised the nanofluid due to the modification of the wettability and altered surface charge of the rock by desorbing the carboxylic group [3].

Therefore, after nanofluid injection, it was much easier for the aqueous phase to enter the porous medium. In another study, a strong magnetic field was applied (via neodymium magnets with strengths up to 6,000 G) first, followed by Fe_2O_3 (concentrations ranged from 0.01 to 0.02 wt% mixed in DW and SW) nanofluid injection, yielding a zeta potential of -14.4 mV and -15.1 mV, respectively, and contact angles of 46° and 37° [28]. When an EH was added before the imbibition of 0.0025 wt% MgO NPs mixed in DW (**core #5** and **core #6**), the contact angle and zeta potential measurements suggested a significant reduction from 123.8° to 69° and from -24.4 mV to -25,48 mV from **core #5**, and from 123.8° to 65° and from -24.4 mV to -28.3 mV from **core #6**. The magnetic field generated from the EH was calculated from the coil parameters (inner radius (mm), coil length (mm), copper wire diameter with the insulation (mm), copper diameter without the insulation (mm), number of turns, and coil current (A)). Other parameters were taken as default values such as frequency (1 kHz), distance from the centre (0 mm), core relative permeability (1), and winding compaction factor (1) [29].

If we compare the magnetic field strength used in previous experiments for the Amott cells using a magnetic field of 6,000 G with 27 magnets and the one generated from the EH [3] is only 20 mT (200 G) generated from 30 V. Hence, the difference is 810 times.

Thus, even though electricity produced an MF that was 810 times weaker than that produced by neodymium magnets [10], at high voltage, the combined effect of heat and the magnetic field caused lower zeta potential magnitude and contact angle values, indicating a shift in wettability. The electric field also changed the electro-rheological properties, for instance, the viscosity of the displacing fluid increased [19].

Porosity values correlated with the contact angle and zeta potential values (**Table 5**), indicating that this hybrid technique enhances flow in porous media better than neodymium magnets combined with NPs, because of the effect of heating and the electric field. The likely mechanism is electrowetting [3,27]. Electrowetting is defined by the change of wettability under the effect of the electrical field caused by electrical heating [30].

3.2. Spontaneous imbibition tests

Spontaneous imbibition tests were carried out to study the impacts of Fe_2O_3, and MgO nanofluid on oil recovery and their combination with EH on interfacial tension and pH values.

3.2.1 Impact of Fe_2O_3 NPs on oil recovery

Fig. 4 demonstrates oil recovery from oil-wet Austin chalk imbibed with a solution of Fe_2O_3 NPs in DW and SW, before and after the introduction of EH.

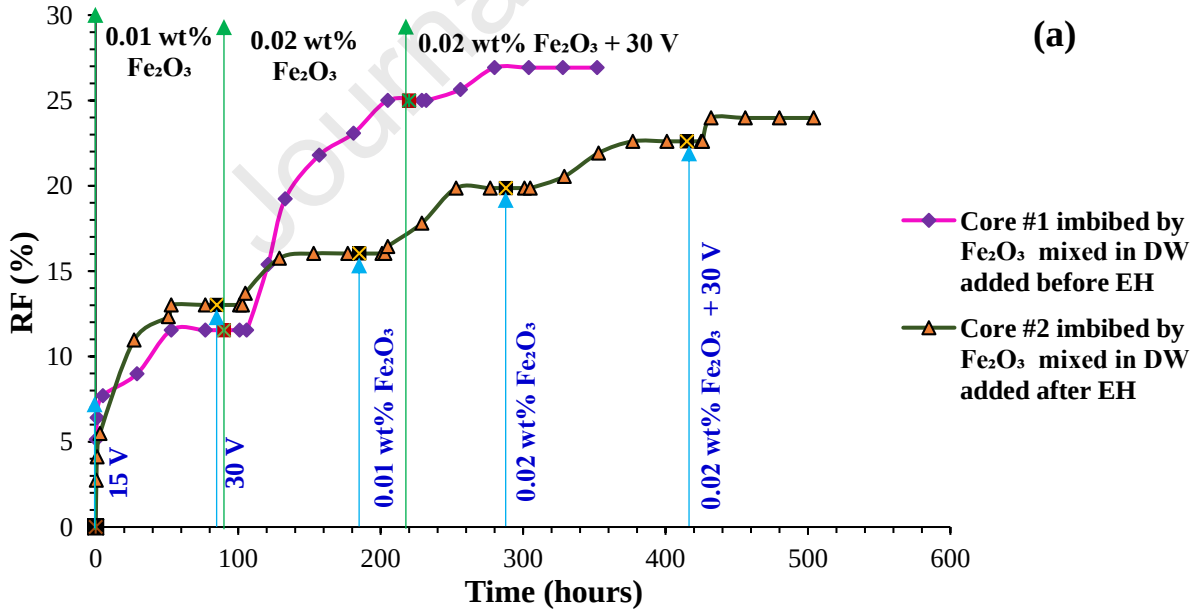

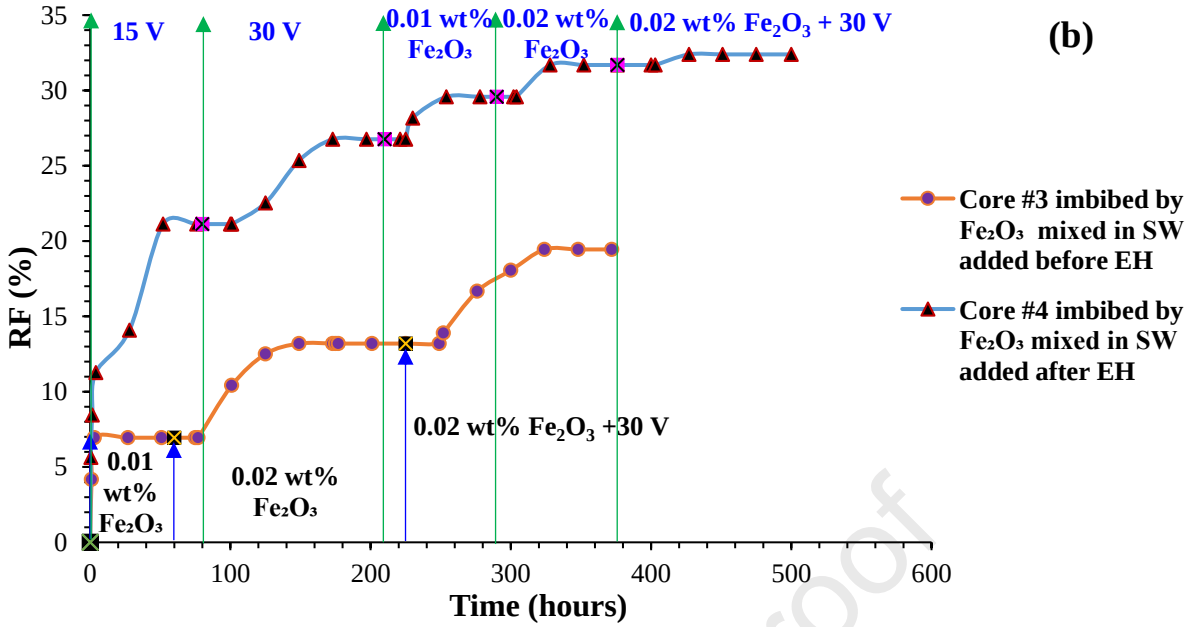

Fig. 4. Effect of Fe_2O_3 NPs in (**a**) DW and (**b**) SW (before and after introducing an EH) on oil recovery from initially oil-wet chalk samples.

Fig. 4 (a) displays oil recovery for **core #1** and **core #2**, which were imbibed by a solution of Fe_2O_3 NPs in DW before and after EH was introduced. When 0.01 wt% and 0.02 wt% Fe_2O_3 NPs were added at the start of the spontaneous nanofluid imbibition followed by EH (**core #1**), oil recovery increased from 2.9% to 11.5% and 25.0%, respectively. Adding 30 V further increased oil recovery by 1.9%, increasing it to 26.9% in total. In **core #2**, however, ultimate oil recovery increased to 13.0% and 16.0% after applying 15 V and 30 V at the beginning of the spontaneous imbibition.

When 30 V were applied after 0.02 wt% Fe_2O_3 nanofluid was introduced, RF increased by 1.4%, resulting in 24.0% total oil recovery. Similar tests revealed that Fe_2O_3 NPs increased oil recovery by 25 % [28] and that the oil recovery increased from 25.0% to 27.9%, 6,000 G were added to the Fe_2O_3 nanofluid by 27 neodymium magnets [28]. This indicates that NPs perform better when added at the beginning of the imbibition, as the nanofluids alter the surface charge and the wettability of the rock very efficiently (compared with EH alone).

The imbibition results for the cores imbibed by Fe_2O_3 NPs in SW are displayed in **Fig. 4 (b)** before (**core #3**) and after (**core #4**) adding EH. When SW was introduced at the start of spontaneous imbibition, oil recovery was 11.5%. However, when 0.01 wt% and 0.02 wt % Fe_2O_3 NPs mixed in SW

were introduced at the beginning of the imbibition (**core #3**), RF was 13.1%, with just a 1.4% increase when compared with SW alone. This marginal increase can be attributed to the low stability of the Fe_2O_3 nanofluid [31]. The oil recovery increased by 6.3% when 30 V were applied to 0.02 wt % Fe_2O_3 NPs mixed in SW, implying that the EH enhanced sulphate adsorption on the rock surface, which in turn enhanced the suspension stability of the magnetised NPs via repulsive Van der Waals forces of the upper paramagnetic Fe_2O_3 NPs, which enhances the interaction with the MF and improves the suspension stability [32]. Furthermore, pore throats are weakly or not blocked in case of improved suspension stability, which can be achieved by adding EH or an MF (poor invasion of the NPs mixed in SW into the porous medium was caused by pore throat clogging) [33].

Pre-magnetisation, when combined with EH-preheating, resulted in higher sulphate adsorption, and consequently a shift in rock surface charge, and contact angle, and thus in improved suspension stability and invasion of the Fe_2O_3 nanofluid. When Fe_2O_3 NPs mixed in DW/SW were added at the beginning of spontaneous imbibition, higher oil recovery was achieved (1% extra). EH, introduction resulted in higher oil recovery, even though the productivity of the SW-based nanofluid was lower than that of the DW-based nanofluid (due to poor NP suspension stability and core invasion). Thus, a higher oil recovery was achieved with SW alone (25%) due to a higher rate of sulphate adsorption [34], compared to 19% using neodymium magnets [27]. Note that sulphate occupies the sites on the rock surface (when heated) and desorbs the carboxylic group by ion exchange.

This higher sulphate adsorption rate also altered the rock wettability and reversed surface charge [3,34], allowing for better NP invasion and improved oil production [35,36].

However, applying 15 V, 30 V and (0.01 wt% or 0.02 wt%) Fe_2O_3 NPs mixed in DW/SW, and then exposing the sample to 30 V is more time-consuming (~500 hours total imbibition time –see **Fig. 4**-) than directly using neodymium magnets combined with NPs [28]. However, if only 30 V was applied to the sample initially, followed by the injection of NPs, and then exposed to 30 V again, the imbibition time decreased significantly (~100 hours less, see **Fig. 4**) when magnets were used [3,27].

3.2.2 Impact of MgO NPs on oil recovery

Another series of experiments–similar to those carried out with Fe_2O_3 NPs –were carried out with MgO NPs. Oil recovery data from initially oil-wet cores imbibed by 0.0025 wt% MgO NPs mixed in DW and SW, applied before and after EH is shown in **Fig. 5**.

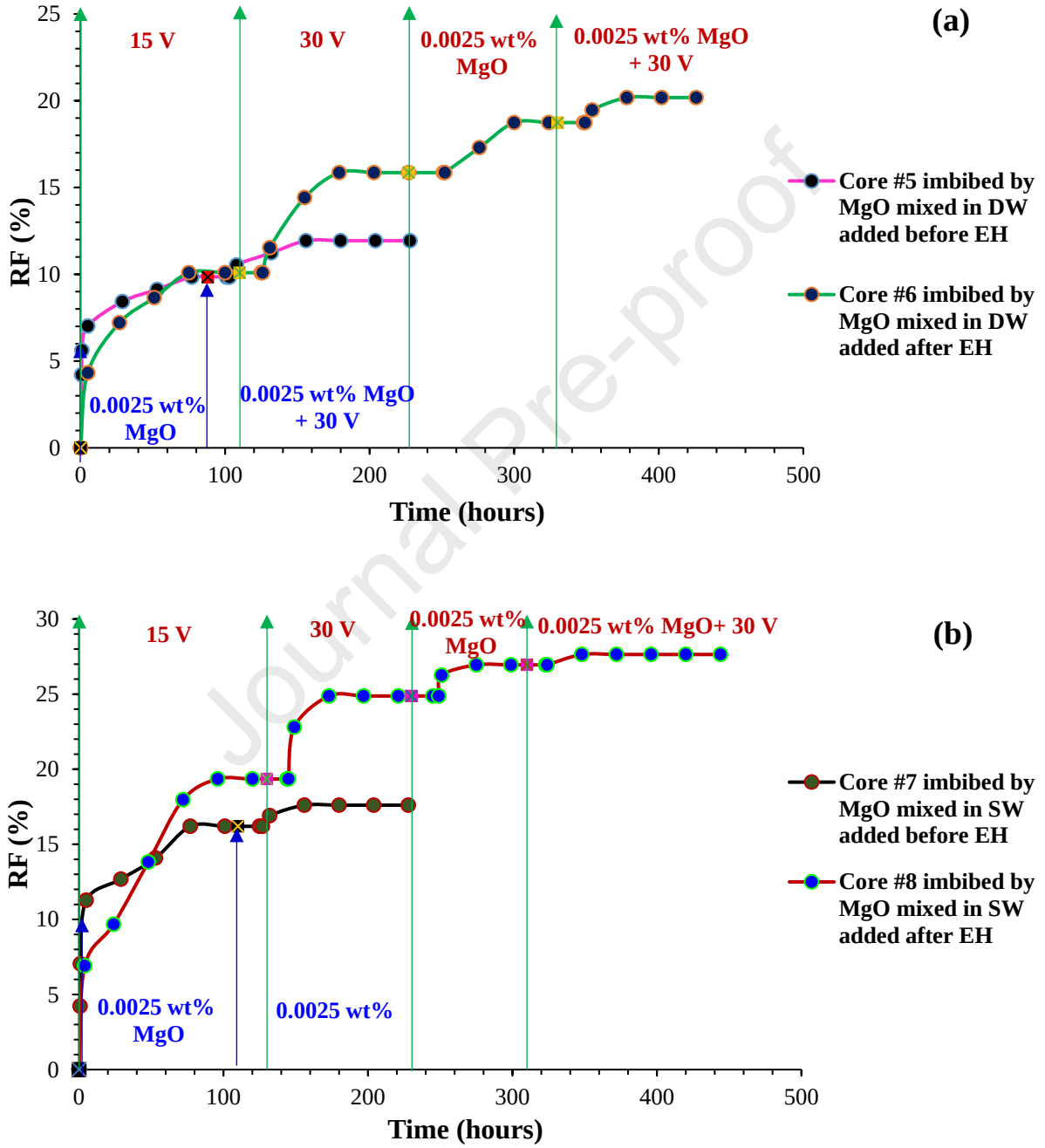

Fig. 5. Effect of MgO NPs suspension in DW (**a**) and SW (**b**) before and after introducing EH on oil recovery from initially oil-wet cores.

296 Flooding with 0.0025 wt% MgO NPs in DW increased oil recovery by 10.1% (**core #5**, **Fig. 5 (a)**).
297 However, oil recovery increased only by 1.8% after EH (of up to 30 V) was applied to the Amott cells
298 after NP application. When an MF was applied first (**core #6** (**Fig. 5 (a)**), followed by MgO NP
299 flooding, an increase in oil recovery of 18.7% (2.9% NPs oil recovery efficiency) was observed. Oil
300 recovery increased further by 1.4% to 20.2%, after adding 30 V. Although the strength of the MF
301 generated by the EH is 810 times lower than that of the neodymium magnets [10], switching from an
302 MF generated at room temperature to EH resulted in a significant increase in oil recovery when SW
303 was used as imbibing fluid (from 19.0% using neodymium magnets to 25.0% using EH [3,27]. This can
304 be attributed to the influence of heat, which aids in the decomposition of carboxylic groups present in
305 the hydrophobic surface layer (sulphate also occupies the rock site and desorbs the oil-see **Fig. 8** and
306 **Fig. 9**). A summary of the oil recovery data is given in **Table 6**.

307

Table 6. Oil recovery data.

		Total RF (%)	**NPs efficiency (%)**	**EH`s efficiency (%)**
Core #1 Fe_2O_3 mixed in DW added before EH	DW	**2.87**	**0**	**0**
	DW+0.01 wt% Fe_2O_3	**11.53**	**8.66**	**0**
	DW+0.02 wt% Fe_2O_3	**24.99**	**13.46**	**0**
	DW+0.02 wt% Fe_2O_3+ 30 V	**26.92**	**0**	**1.93**
Core #2 Fe_2O_3 mixed in SW added before EH	DW+15 V	**13.01**	**0**	**10.14**
	DW+30 V	**16.03**	**0**	**3.01**
	DW+0.01 wt% Fe_2O_3	**19.86**	**3.83**	**0**
	DW+0.02 wt% Fe_2O_3	**22.6**	**2.74**	**0**
	DW+0.02 wt% Fe_2O_3 + 30 V	**23.97**	**0**	**1.37**
Core #3 Fe_2O_3 mixed in DW added after EH	SW	**11.83**	**0**	**0**
	SW+0.01 wt% Fe_2O_3	**6.99**	**-4.84**	**0**
	SW+0.02 wt% Fe_2O_3	**13.19**	**6.2**	**0**
	SW+0.02 wt% Fe_2O_3+ 30 V	**19.44**	**0**	**6.25**
	SW+15 V	**21.12**	**0**	**9.29**

Core #4 Fe_2O_3 mixed in SW added after EH	SW+30 V	**26.75**	**0**	**5.63**
	SW+0.01 wt% Fe_2O_3	**29.57**	**2.82**	**0**
	SW+0.02 wt% Fe_2O_3	**31.68**	**2.11**	**0**
	SW+0.02 wt% Fe_2O_3+ 30 V	**32.39**	**0**	**0.71**
Core #5 MgO mixed in DW added before EH	DW	**2.87**	**0**	**0**
	DW+ 0.0025 wt% MgO	**9.83**	**6.96**	**0**
	DW+ 0.0025 wt% MgO+30 V	**11.93**	**0**	**2.1**
Core #6 MgO mixed in SW added before EH	DW+15 V	**10.09**	**0**	**7.22**
	DW+30 V	**15.85**	**0**	**5.76**
	DW+0.0025 wt% MgO	**18.74**	**2.89**	**0**
Core #7 MgO mixed in DW added after EH	SW	**11.83**	**0**	**0**
	SW+ 0.0025 wt% MgO	**16.19**	**4.36**	**0**
	SW+ 0.0025 wt% MgO+30 V	**17.6**	**1.41**	**0**
Core #8 MgO mixed in SW added after EH	SW+15 V	**19.34**	**0**	**7.51**
	SW+30 V	**24.87**	**0**	**5.53**
	SW+0.0025 wt% MgO	**26.94**	**2.07**	**0**
	SW+0.0025 wt% MgO+ 30 V	**27.63**	**0**	**0.69**

3.2.3 Impact of NPs combined with EH on interfacial tension and pH values

The effect of this hybrid technique (NPs combined with EH) on surface tension and pH value of the imbibing fluid before and after imbibition was investigated. This is discussed in detail below.

a) Impact of NPs on surface tension

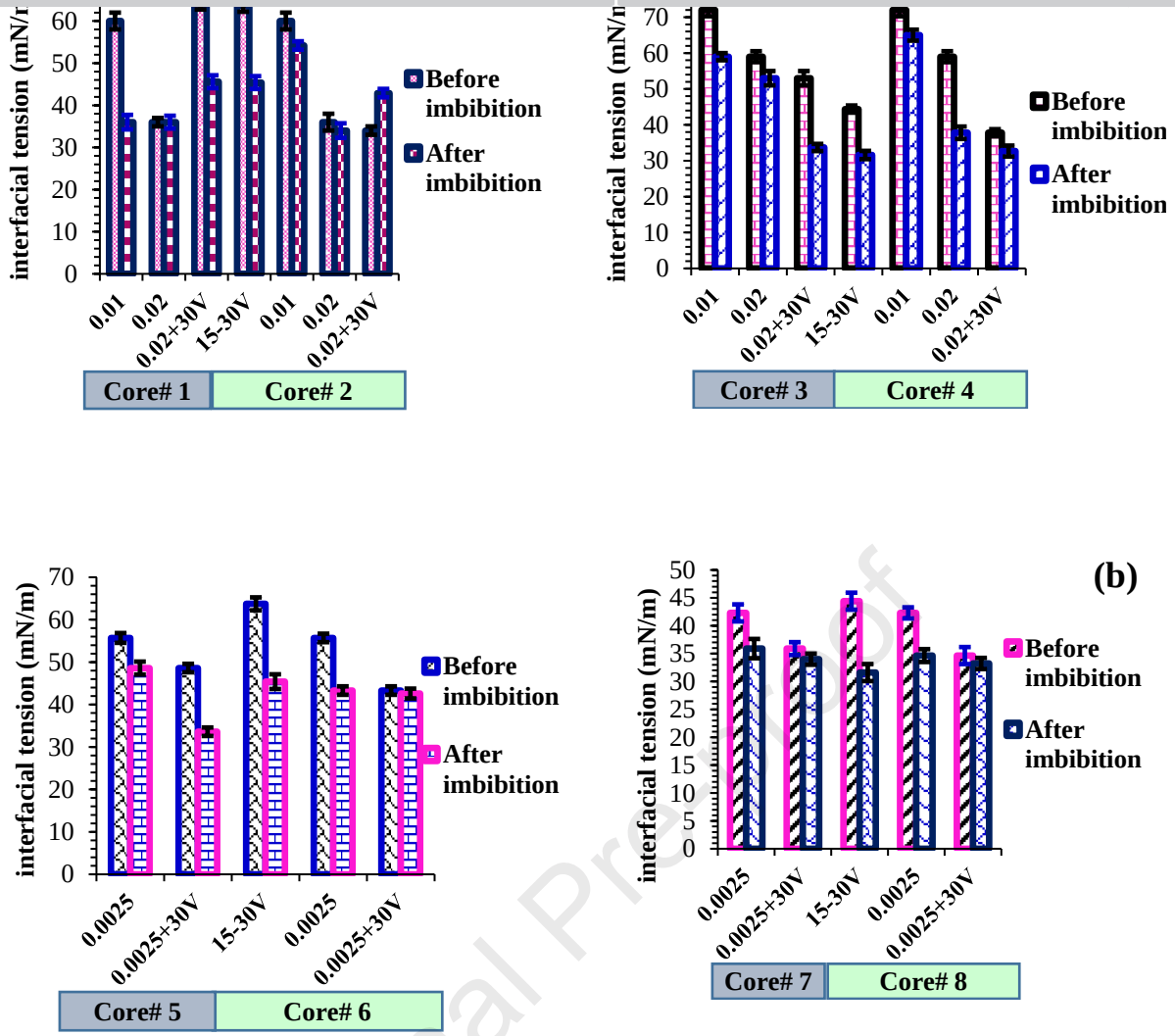

Fig. 6. Effect of NPs paired with EH on the interfacial tension of the aqueous phase, **a)** Fe_2O_3 NPs, **b)** MgO NPs.

The interfacial tension results from **core #1** and **core #2** when Fe_2O_3 NPs mixed in DW were added before and after EH are illustrated in **Fig. 6 (a)**. A reduction in interfacial tension is observed in both cases before and after applying EH; however, a more significant reduction is observed when EH was introduced after Fe_2O_3 NPs were applied - for example, interfacial tension in **core #1** decreased from 63.1 mN/m to 35.8 mN/m. When EH was applied first, and NPs were added afterwards, interfacial tension dropped to 33.9 mN/m (**core #2**). For SW-based nanofluids, the interfacial tension in **core #3** was reduced from 72 mN/m to 33.7 mN/m after EH.

Note that increased temperature within the reservoir lowers interfacial tension and reduces oil viscosity [37,38]. The interfacial tension of Fe_2O_3 NPs mixed in DW, after an MF of up to 6,000 G was applied, decreased from 60 mN/m to 36 mN/m, and from 72 mN/m to 52 mN/m, when Fe_2O_3 NPs were mixed in SW. In contrast, MF (generated by neodymium magnets) did not affect interfacial tension [28].

MgO NPs also had an interfacial-tension-lowering effect, **Fig. 6 (b)**. In **core #8**, for example, there was a greater reduction from 34.7 mN/m to 33.2 mN/m due to the desorption of oil caused by the effect of the pre-magnetisation. It is apparent that adding MgO NPs after applying a voltage of up to 30 V (**core #5** and **core #6**) resulted in a substantial reduction in surface tension. However, this reduction was lower than what was observed for Fe_2O_3 NPs. This discrepancy between MgO and Fe_2O_3 NPs may be attributed to the superparamagnetic aspect of the Fe_2O_3 NPs, or the pre-magnetised SW causing pre-alteration of the rock surface charge, contact angle (and thus better penetration of the Fe_2O_3 NPs), which further decreased the interfacial tension. As a result, NPs decreased the water contact angle, increased the magnitude of the zeta potential, reduced interfacial tension and increased oil production (see **Tables 5**, **6**, and **Figs 4**, and **5**).

b) Impact of NPs on pH value

When NPs were mixed in DW and SW before and after EH, the effect of the nanoparticles on the aqueous phase was measured.

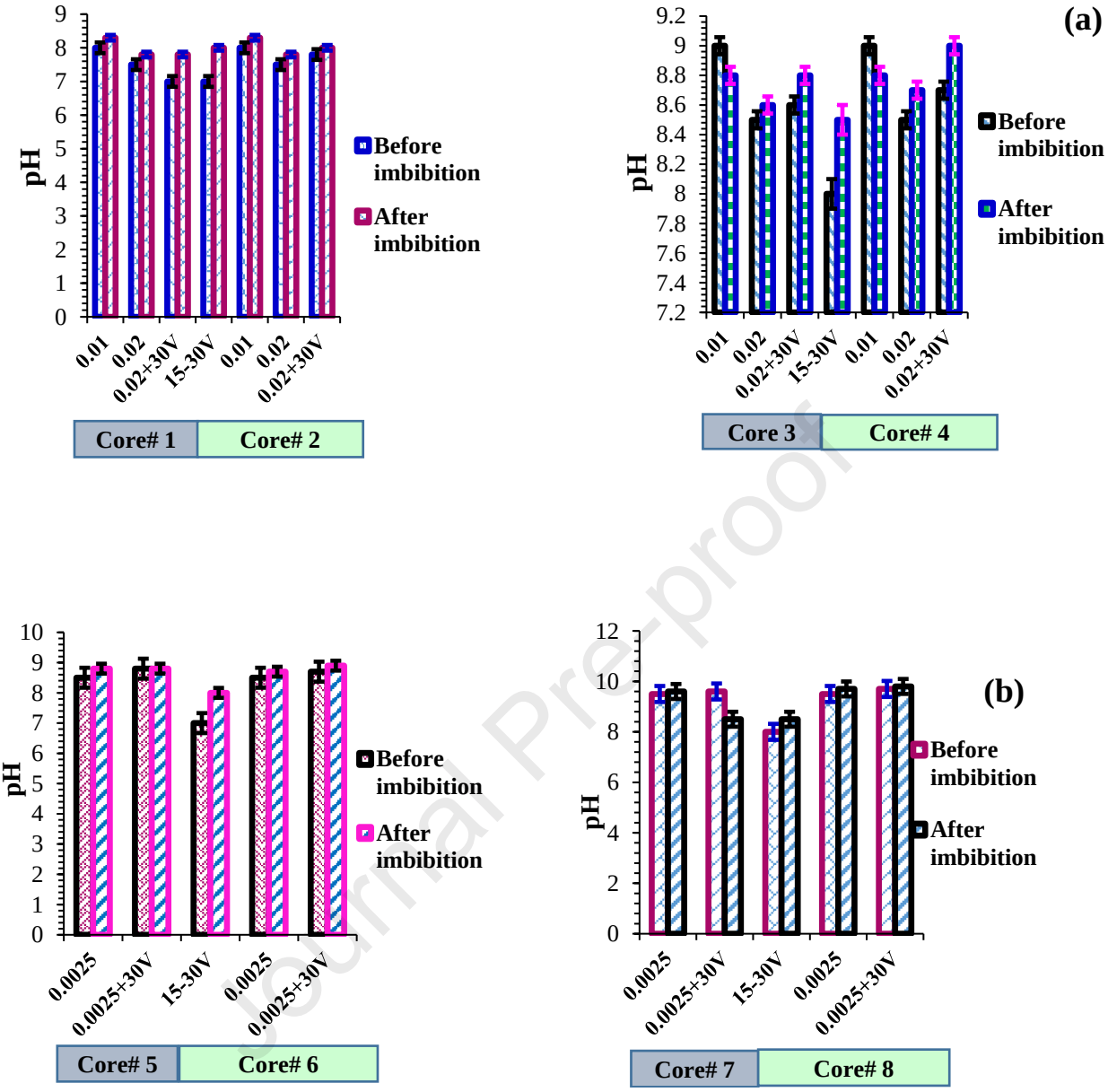

Fig. 7. Effect of NPs paired with EH on the pH of the aqueous phase, **a)** Fe_2O_3 NPs, **b)** MgO NPs.

Fig. 7 shows the influence of Fe_2O_3 NPs and MgO NPs mixed in DW/SW (applied before and after EH) on the pH value. A higher increase in the pH value was observed for Fe_2O_3 NPs (**Fig. 7 (a)**). Changes in the pH value can impact the electrical charges on the carbonate rock surfaces, resulting in a wettability change [39,40]. Here, pH increased after spontaneous imbibition. In **core #1 (Fig 7. (a))**, for example, when 15-30 V were applied at the start, pH increased by unity, and when 0.01-0.02 Fe_2O_3 wt% and 15-30 V were added, pH increased by 0.3 and 0.2, respectively. As a result, starting with EH

has a substantial effect on the rise in pH, resulting in a high oil recovery. This is consistent with the oil production, zeta potential, and contact angle results. Further improvement (in oil recovery) was found for the SW systems (**core #3**) and (**core #4**) (**Fig. 4**); this can be attributed to the fact that EH increases sulphate adsorption (SO_4^{2-}), see above. However, as pre-magnetisation and pre-heating were applied at the start of the process, it resulted in a higher pH value, because SW combined with EH altered the rock surface properties by reversing the surface charge and reducing the contact angle by electrowetting [3], **Table 5**, as well as decreasing the interfacial tension, **Fig. 6**. Pre-magnetisation allowed the modification of wettability and zeta potential before the incorporation of NPs; pre-magnetisation thus boosted NP penetrability into the porous medium and increased oil recovery [3]. Similar results were obtained with MgO NPs, where a further rise in oil recovery was found for the SW systems. However, a transition was observed with Fe_2O_3 NPs, perhaps due to their ferromagnetic nature –Fe_2O_3 interacts more strongly with the generated MF [28]- which improved suspension stability even in a SW environment [32,41]. Combining an MF with Fe_2O_3 or Al_2O_3 NPs resulted in a decrease in interfacial tension (a greater decrease was observed with Fe_2O_3 NPs) - this is attributed to higher desorption of carboxylic groups induced by the added heat [28]. Furthermore, Fe_2O_3 has a higher surface area and surface-to-volume ratio due to its superparamagnetic nature [32,41]. However, an MF on its own had little effect on interfacial tension, probably due to the low temperature applied [3]. When Fe_2O_3 and MgO NPs were combined with EH (**Fig. 7 (a)**) similar effects on pH [28] were observed. Fe_2O_3 NPs reduced interfacial tension (**Fig. 6 (a)**), and increased pH (**Fig. 7 (a)**) more than MgO NPs.In contrast to MF, EH noticeably reduced surface tension (before and after NP application), due to the heat added, which also correlated with a small increase in oil recovery. Furthermore, owing to variations in magnetisation properties, MgO NPs (paramagnetic) outperformed Al_2O_3 (NPs non-magnetised) [10].

4. Mechanism of the hybrid technique (using NPs in combination with EH)

Previous studies on magnetic fields, EH, and hybrid methods involving magnets and NPs have been performed [42–44]. To get a better understanding of the mechanisms occurring in oil-wet carbonate reservoirs, we hypothesise multiple mechanisms, **Fig. 8** and **9**.

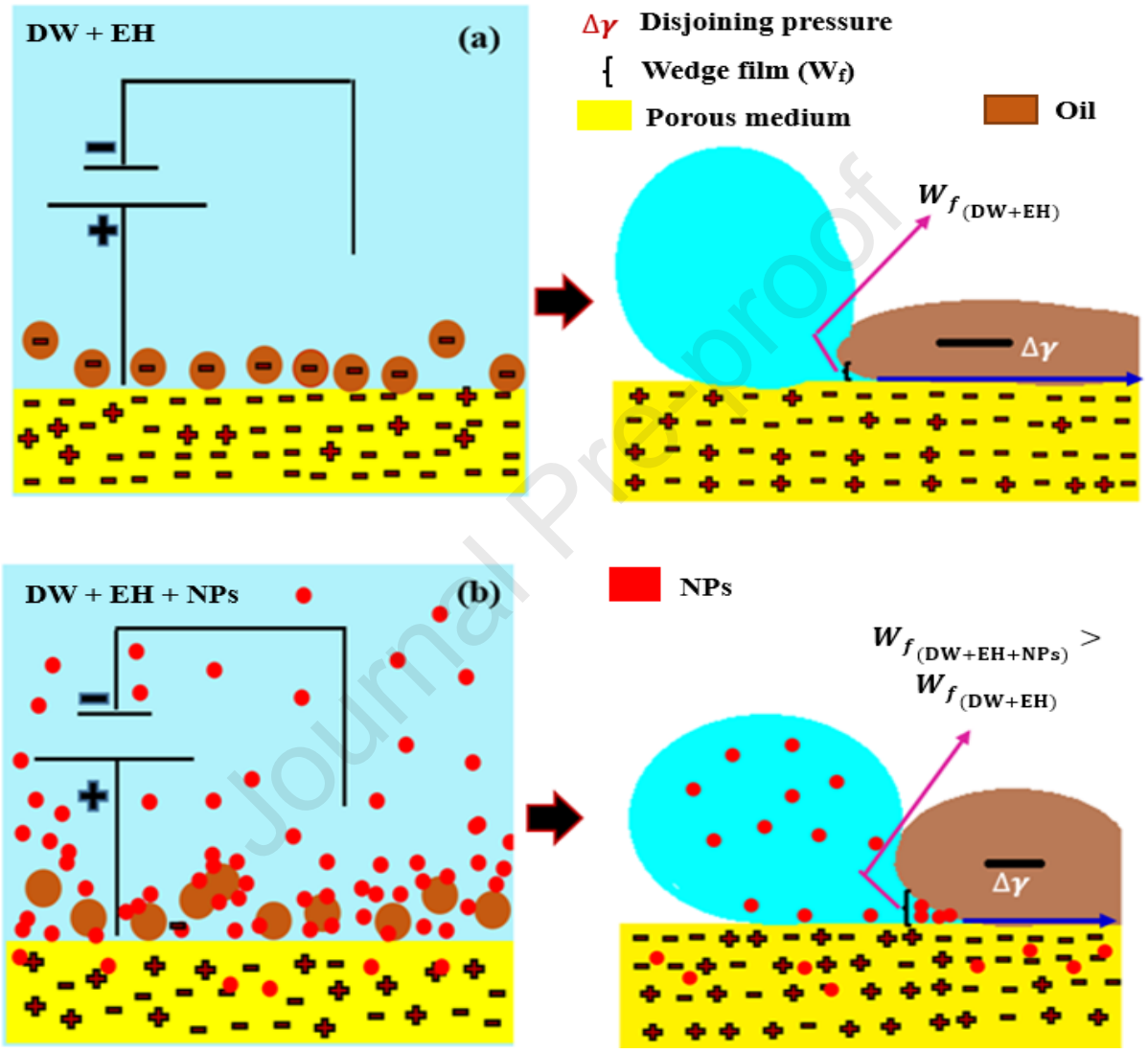

Fig. 8. Hypothesised mechanisms of the hybrid technique (EH combined with NPs) when the DW was pre-magnetised, and NPs were added afterwards **a)** DW+ EH, **b)** DW+ EH +NPs.

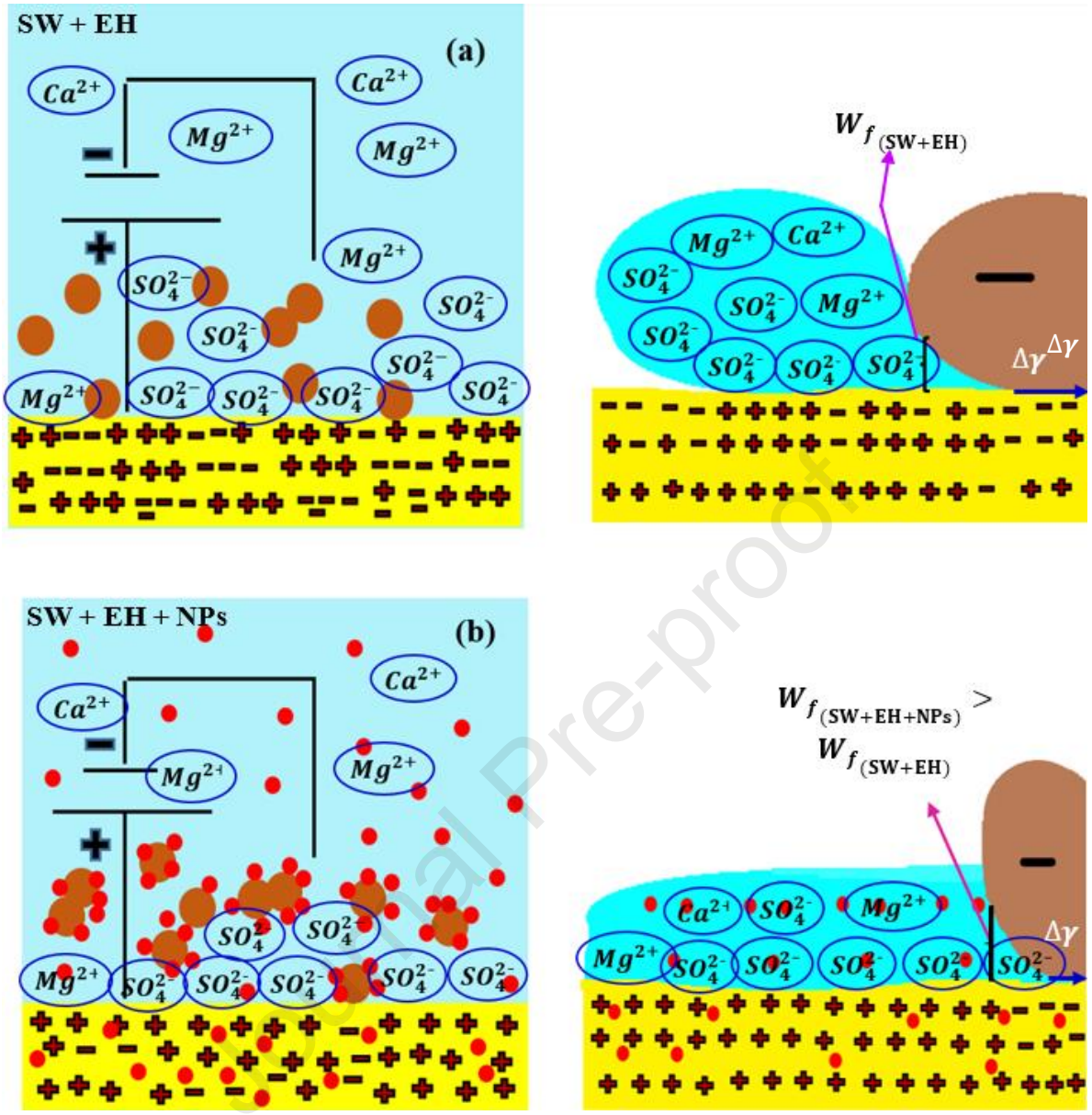

391

392 **Fig. 9.** Hypothesised mechanisms of the hybrid technique (EH combined with NPs) when the DW was pre-
393 magnetised, and NPs were added afterwards **a)** SW+ EH, **b)** SW+ EH +NPs.

394

395 When the solution was pre-magnetised (with or without NPs), higher and earlier oil production could
396 be achieved [11,27,28]. As a result, our proposed mechanism is built on pre-magnetisation followed by
397 NP injection. We therefore hypothesise that EH-assisted nanofluid flooding is related to a reduction in
398 interfacial tension and wettability alteration [45–47].

399 The processes depicted in **Fig. 8** and **9** are based on experimental measurements for pH values,
400 interfacial tensions, contact angles, and zeta potentials; and the proposed mechanism primarily depends

on the hybrid technique's combined impact on electrowetting and disjoining pressure (pre-heating and NPs). Due to the cumulative action of magnetisation and heating, electrowetting causes a change in wettability under the influence of electricity, allowing a water droplet on the rock surface to flatten, with an increase in drop width and a decrease in height, indicating a more hydrophilic state [3]. Furthermore, NP (water-wet NP) adsorption on the rock surface further reduces rock hydrophobicity [48,49]. Electrowetting, which is caused by electric stimulation, is a good way to modify the surface wettability and deform the shapes of oil droplets; while electrowetting can also reduce imbibition time [50,51].

Fig. 8 demonstrates the mechanisms involved in the hybrid technique when DW is injected at the start of spontaneous imbibition (before NPs are added). Oil droplet detachment is caused by a rise in the height of the water wedge film of water, W_f, due to increased disjoining pressure [28]. For instance, oil recovery with EH (up to 30 V, in **core #2**, **Fig. 4**) was 16.0 %, which is 13.2% higher than that without EH (2.9%) and two times higher than with an MF (162,000 strength) (6.8%) [27,28]. Oil recovery increased by 6.6% to 24.0% after adding 0.01-0.02 wt% Fe_2O_3 NPs and after turning off the DC power and turning it back on later and again applying 30 V (**Fig. 4 (a)** and **Table 6**); which was however lower than for MF (162,000 strength) coupled with Fe_2O_3 NPs mixed in DW (27.9%).

When pre-magnetised SW was added before NPs in SW, EH increased sulphate adsorption on the rock surface (**Fig. 9**). As a result, oil desorption increased, and oil production increased to 24%-25%. EH was more effective for SW than DW, resulting in a 14.6% improvement in oil recovery in SW versus 10.6% in DW, **Table 6**.

Furthermore, during pre-magnetisation, the amplitude of the zeta potential decreased (this was more noticeable with SW; **Table 5**) and became less negative for Fe_2O_3 NPs pre-magnetisation removed negatively charged carboxyl groups in the oil. When MgO NPs were mixed in DW or SW, the zeta potential became more negative (it decreased from its initial negative value of -5 mV to -28.4 mV (MgO NPs mixed in SW added before EH -**core #6**-) and -32.9 mV (MgO NPs mixed in SW added after EH

426 - **core #8**), respectively; see **Table 5**), implying a better penetration of the NPs into the porous medium
427 after pre-magnetisation.

428 This suggests that MgO NPs in DW are more efficient in rendering the rock surface charges more
429 negative. The interfacial tension of the aqueous phase (with/without Fe_2O_3/MgO NPs) decreased by the
430 pre-magnetisation and the pre-heating due to the EH added at the beginning of the spontaneous
431 imbibition the NPs added later, **Figs. 6 (a)** and **(b)**; also the pellet porosity increased (from 6.6 to 12.7%)
432 when SW was used, consistent with contact angle decrease (from 123.8^o to 62^o) and zeta potential
433 magnitude increase (from -24.4 to -27.0 mV). When NPs were mixed in SW, pre-magnetisation of the
434 SW resulted in higher oil recovery, due to changes in wettability and surface charge, allowing improved
435 NP invasion and expansion of the wedge film. As a result, the water droplet was flatter than in the case
436 of DW. The wedge film produced by EH with/without NPs was also likely thicker than that produced
437 by neodymium magnets (with/without NPs).

438 EH sped up SW imbibition and the contact angle decline time in the presence and absence of the MF
439 generated by the EH/Neodymium magnets (in comparison to DW), which in turn was more than MF
440 generated by the neodymium magnets. This would be due to the combined effect of the heat and MF
441 even though the MF generated by EH is 810 times lower than the one generated by the neodymium
442 magnets [3,52]. However, imbibition slowed down (**Figs. 4** and **5)** when EH sequences (15 V then 30
443 V) were applied. Furthermore, nanofluids should have been injected while DC power is applied.

444 To describe the relationship between oil production rate and disjoining pressure, Δt (defined as the time
445 required to extract an oil droplet before and after introducing any EOR technique) was examined [28]
446 and was concluded that:

447 $$\Delta t_{WF} < \Delta t_{FB} < \Delta t_{SW} < \Delta t_{mag} < \Delta t_{mag+NPs} \quad (1)$$

448 where $\Delta t_{WF}, \Delta t_{FB}, \Delta t_{SW}, \Delta t_{mag}, \Delta t_{mag+NPs}$ represent Δt for normal water flooding without potential
449 determining ions (PDIs) (Δt_{WF}), formation brine (Δt_{FB}), seawater/smart water (Δt_{SW}), magnets
450 (Δt_{mag}), and magnet-assisted nanofluids ($\Delta t_{mag+NPs}$), respectively.

451 It was found that EH accelerates the decline in contact angle decline and the onset of imbibition
452 compared to an applied MF, due to the increase in temperature caused by EH [3], hence, Eq. (1) can be
453 developed further to:

454 $$\Delta t_{SW+EH} > \Delta t_{SW+EH+NPs} > \Delta t_{SW+MF} > \Delta t_{SW+MF+NPs} > \Delta t_{SW} > \Delta t_{FB} > \Delta t_{WF} \quad (2)$$

455 This equation corresponds to the wedge film (W_f) generated by the disjoining pressure.

456 $$W_{f(SW+EH)} > W_{f(SW+EH+NPs)} > W_{f(SW+MF)} > W_{f(SW+MF+NPs)} > W_{f(SW)} > W_{f(FB)} > W_{f(WF)} \quad (3)$$

457 where Δt_{SW+EH} represents the difference in time needed for oil removal from pre-magnetised SW
458 (direct application of 30 V), $\Delta t_{SW+EH+NPs}$ represents Δt from pre-magnetisation combined with NPs,
459 Δt_{SW+Mag} represents pre-magnetised SW, $\Delta t_{SW+Mag+NPs}$ represents pre-magnetised SW-nanofluid
460 (with NPs), Δt_{SW} represents SW or smart water flooding, Δt_{FB} represents formation brine, and Δt_{WF}
461 represents normal water flooding (or DW).

462

463 ## 5. Suggestions for field application

464 **Fig. 10** presents a schematic of a field-scale application where electrical heating is used.

465

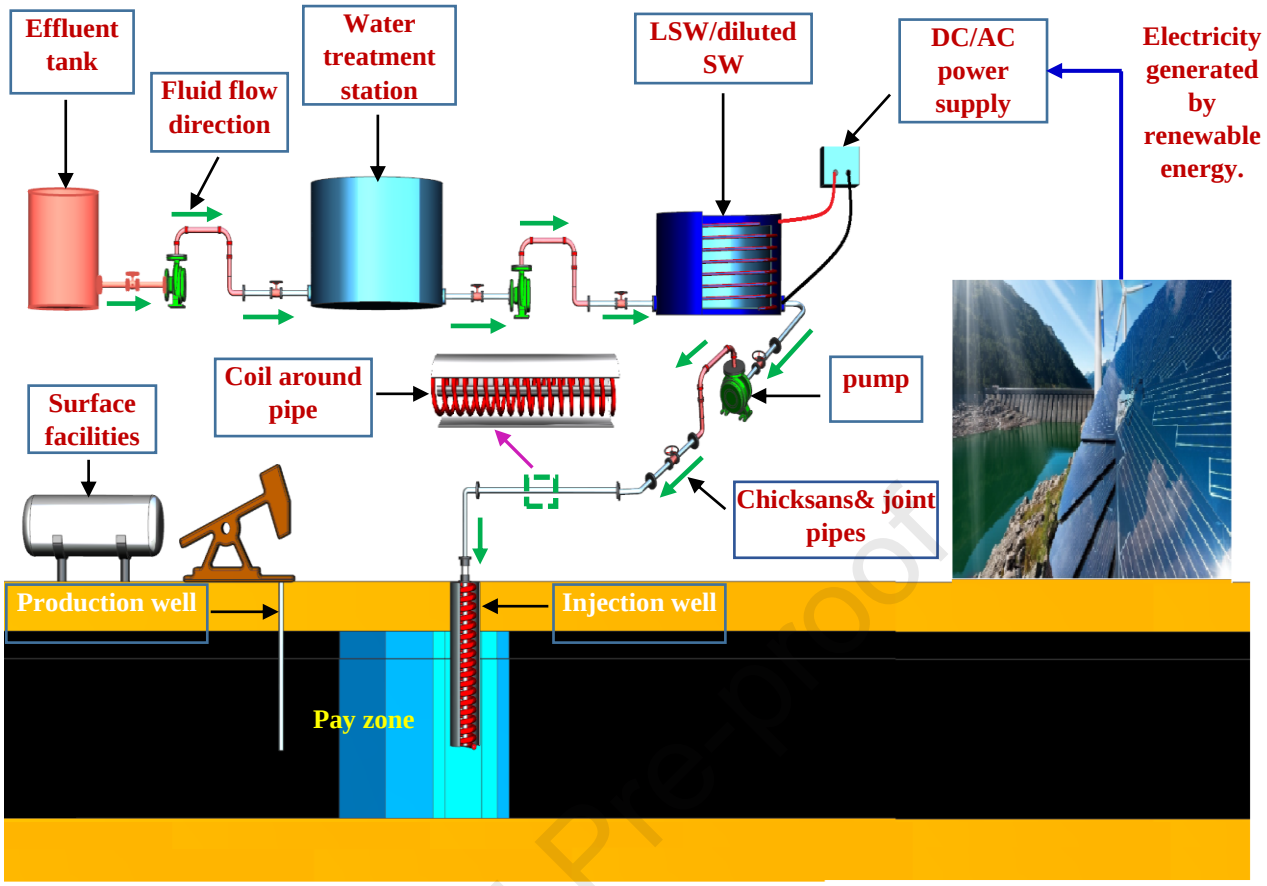

Fig. 10. Field-scale application of electrical heating to improve oil recovery.

Electrical heating can be a cleaner technique to enhance oil recovery, minimising pollution through chemicals [53], especially when green electricity is used [54]. Technically, produced water is collected in an effluent tank and supplied to a water treatment station for purification (note that electric fields can also have a great impact on water treatment) [55,56]. Hence, coiled tubing and external piping are added to the storage tank to ensure continuous flow operations under controlled operations of flow, level, and temperature. The purified water is used to prepare low-salinity water by dilution. The SW tank is equipped with a coil which is connected to a power supply to generate electrical, ensuring preheating and pre-magnetisation of the SW before injection. However, this can be costly as a special design is required. Furthermore, this tank should be equipped with a level-controlled indicator and a thermostat which sets a maximum temperature (~40C^{o}) for water losses by evaporation. The heated and magnetised low salinity water is then ready to be injected into the wellhead while the NP tank should be placed just after the diluted SW tank.

To save costs, it is advised that measures be taken to avoid the evaporation of SW and prevent overheating. Furthermore, coils around the SW tank should be eliminated, and only pipes in the pay zone should be dotted with coils for high-temperature formations. Also, electrification of the equipment for net zero targets and cost optimisation is required, while the system can be optimised by adding coils to the pipes of the LSW/diluted SW tank`s discharge pump closer to the wellhead, similar to what has been suggested previously for magnetised nanofluid flooding [28].

Field-scale electrical heating can be carried out with a process control strategy, including a simple On/Off electric supply with a defined frequency for controlled production rates [57]. However, an economic study is required to assess the economic potential of this technique, and a special piping design (two layers with a coil in between) is required to fit the coils inside.

6. Summary and Conclusions

The following conclusions were drawn when comparing the hybrid methods (EH combined with NPs versus MF combined with NPs):

- The rock zeta potential of chalk samples imbibed with nanofluid at the end of spontaneous imbibition depended on the NPs' initial zeta potential. Electrical heating enhanced ion desorption and adsorption, rendering the zeta potential more negative when compared with similar experiments when a higher magnetic field was imposed without heating.
- Due to enhanced sulphate adsorption (caused by heating) [58], pre-heated and pre-magnetised nanofluids yielded higher oil recoveries than magnetised nanofluids.
- Fe_2O_3 NPs provided the highest oil recoveries of all the hybrid options.
- Heat lowered the interfacial tension of the imbibing fluid and caused decarboxylation, altering the surface charge of the rock, and thus reducing oil wetness and contact angle.

Although imbibition was slower when electricity was introduced first due to several steps (15 V, 30 V, NPs, then NPs + 30 V), however, the ultimate oil recovery was superior. Moreover, Fe_2O_3 NPs reduced the water contact angle (39^o for DW, and 36^o for SW) more than MgO NPs (54^o for DW and 52^o for

506 SW) when NPs were added after EH. This was due to the pre-magnetisation and pre-heating.
507 Furthermore, heat proved to accelerate imbibition more than the MF generated by neodymium magnets.
508 Hence, the imbibition time was further reduced for the EH-nanofluid hybrid technique when 30 V were
509 applied at the start of the imbibition. The EH-nanofluid hybrid technique enabled higher oil production
510 in a shorter time compared with the MF neodymium magnets-nanofluid hybrid, thus improving oil
511 recovery and securing energy supply.

512 This work guides towards the combined use of electrical heating and nanoparticles for EOR, although
513 scale-up activities, field-scale pilot studies and techno-economic analyses are needed. In summary, the
514 method is very promising for the improvement of the recovery in the near injection-well region, with
515 effects throughout the pay zone, particularly on onshore fields with close well spacing.

516

517 **Acknowledgement**

518 The authors express their gratitude to the University of Teesside, UK for facilitating and funding the
519 tests vital to this research.

520

References

[1] Mousumi Roy, Sustainable Development Strategies Engineering, Culture and Economics, 2020. https://doi.org/https://doi.org/10.1016/C2018-0-00100-0.

[2] B. Fattouh, R. Poudineh, R. West, The rise of renewables and energy transition: what adaptation strategy for oil companies and oil-exporting countries?, Research Report (2018).

[3] F. Amrouche, D. Xu, M. Short, S. Iglauer, J. Vinogradov, M.J. Blunt, Experimental study of electrical heating to enhance oil production from oil-wet carbonate reservoirs, Fuel 324 (2022) 124559. https://doi.org/10.1016/j.fuel.2022.124559.

[4] G. Dordzie, M. Dejam, Enhanced oil recovery from fractured carbonate reservoirs using nanoparticles with low salinity water and surfactant: A review on experimental and simulation studies, Adv Colloid Interface Sci 293 (2021) 102449. https://doi.org/10.1016/J.CIS.2021.102449.

[5] N. Lashari, T. Ganat, Emerging applications of nanomaterials in chemical enhanced oil recovery: Progress and perspective, Chin J Chem Eng 28 (2020) 1995–2009. https://doi.org/10.1016/J.CJCHE.2020.05.019.

[6] M. Mozafari, Z. Nasri, Operational conditions effects on Iranian heavy oil upgrading using microwave irradiation, J Pet Sci Eng 151 (2017) 40–48. https://doi.org/10.1016/j.petrol.2017.01.028.

[7] F. Bottazzi, C. Repetto, E. Tita, G. Maugeri, Downhole Electrical Heating for Heavy Oil Enhanced Recovery: A Successful Application in Offshore Congo, in: International Petroleum Technology Conference, IPTC 2008, IPTC, 2013. https://doi.org/10.2523/IPTC-16858-Abstract.

[8] B. Hascakir, T. Babadagli, S. Akin, Experimental and Numerical Modeling of Heavy-Oil Recovery by Electrical Heating, in: SPE International Thermal Operations and Heavy Oil Symposium, SPE, 2008: pp. 755–768. https://doi.org/10.2118/117669-MS.

[9] H. Hassanzadeh, T. Harding, Analysis of conductive heat transfer during in-situ electrical heating of oil sands, Fuel 178 (2016) 290–299. https://doi.org/10.1016/j.fuel.2016.03.070.

[10] F. Amrouche, M.J. Blunt, S. Iglauer, M. Short, T. Crosbie, E. Cordero, D. Xu, Using magnesium oxide nanoparticles in a magnetic field to enhance oil production from oil-wet carbonate reservoirs, Mater Today Chem 27 (2023) 101342. https://doi.org/10.1016/j.mtchem.2022.101342.

[11] E. Esmaeilnezhad, S. Le Van, B.H. Chon, H.J. Choi, M. Schaffie, M. Gholizadeh, M. Ranjbar, An experimental study on enhanced oil recovery utilizing nanoparticle ferrofluid through the application of a magnetic field, Journal of Industrial and Engineering Chemistry 58 (2018) 319–327. https://doi.org/10.1016/j.jiec.2017.09.044.

[12] M. Mansouri Zadeh, F. Amiri, S. Hosseni, R. Ghamarpoor, Synthesis of colloidal silica nanofluid and assessment of its impact on interfacial tension (IFT) and wettability for enhanced oil recovery (EOR), Sci Rep 14 (2024) 325. https://doi.org/10.1038/s41598-023-51038-8.

[13] S.S. Sze Lim, H. Elochukwu, J. Nandong, Z. Bennour, M.A. Hamid, A review on the mechanisms of low salinity water/surfactant/nanoparticles and the potential synergistic

application for c-EOR, Petroleum Research 8 (2023) 324–337. https://doi.org/10.1016/j.ptlrs.2023.02.001.

[14] A. Juyal, D. Singh Bhadauriya, R. Sharma, B. Deka, Recovery of heavy crude oil with electrical enhanced oil recovery using lignin nanoparticles: A review, Mater Today Proc (2023). https://doi.org/10.1016/j.matpr.2023.07.110.

[15] K. Guo, H. Li, Z. Yu, In-situ heavy and extra-heavy oil recovery: A review, Fuel 185 (2016) 886–902. https://doi.org/10.1016/j.fuel.2016.08.047.

[16] H. Panchal, H. Patel, J. Patel, M. Shah, A systematic review on nanotechnology in enhanced oil recovery, Petroleum Research 6 (2021) 204–212. https://doi.org/10.1016/j.ptlrs.2021.03.003.

[17] R. Hosny, A. Zahran, A. Abotaleb, M. Ramzi, M.F. Mubarak, M.A. Zayed, A. El Shahawy, M.F. Hussein, Nanotechnology Impact on Chemical-Enhanced Oil Recovery: A Review and Bibliometric Analysis of Recent Developments, ACS Omega 8 (2023) 46325–46345. https://doi.org/10.1021/acsomega.3c06206.

[18] R. Gharibshahi, M. Omidkhah, A. Jafari, Z. Fakhroueian, Hybridization of superparamagnetic Fe3O4 nanoparticles with MWCNTs and effect of surface modification on electromagnetic heating process efficiency: A microfluidics enhanced oil recovery study, Fuel 282 (2020) 118603. https://doi.org/10.1016/J.FUEL.2020.118603.

[19] M.S. Alnarabiji, N. Yahya, S. Nadeem, M. Adil, M.K. Baig, O. Ben Ghanem, K. Azizi, S. Ahmed, B. Maulianda, J.J. Klemeš, K.A. Elraies, Nanofluid enhanced oil recovery using induced ZnO nanocrystals by electromagnetic energy: Viscosity increment, Fuel 233 (2018) 632–643. https://doi.org/10.1016/j.fuel.2018.06.068.

[20] M. Rabiei Faradonbeh, H. Hassanzadeh, T. Harding, Numerical simulations of bitumen recovery using solvent and water assisted electrical heating, Fuel 186 (2016) 68–81. https://doi.org/10.1016/j.fuel.2016.08.077.

[21] E. Esmaeilnezhad, H.J. Choi, Polyindole nanoparticle-based electrorheological fluid and its green and clean future potential conformance control technique to oil fields, J Clean Prod 231 (2019) 1218–1225. https://doi.org/10.1016/j.jclepro.2019.05.341.

[22] H.M. Zaid, N.R.A. Latiff, N. Yahya, H. Soleimani, A. Shafie, Application of electromagnetic waves and dielectric nanoparticles in enhanced oil recovery, Journal of Nano Research 26 (2014) 135–142. https://doi.org/10.4028/www.scientific.net/JNanoR.26.135.

[23] A. Bera, T. Babadagli, Status of electromagnetic heating for enhanced heavy oil/bitumen recovery and future prospects: A review, Appl Energy 151 (2015) 206–226. https://doi.org/10.1016/J.APENERGY.2015.04.031.

[24] E. Esmaeilnezhad, H. Jin Choi, M. Schaffie, M. Gholizadeh, M. Ranjbar, S. Hyuk Kwon, Rheological analysis of magnetite added carbonyl iron based magnetorheological fluid, J Magn Magn Mater 444 (2017) 161–167. https://doi.org/10.1016/j.jmmm.2017.08.023.

[25] K. Zhou, X. Zhou, J. Liu, Z. Huang, Application of magnetic nanoparticles in petroleum industry: A review, J Pet Sci Eng 188 (2020) 106943. https://doi.org/10.1016/j.petrol.2020.106943.

[26] F. Amrouche, S.R. Gomari, M. Islam, D. Xu, Effect of Magnetic Field on Physiochemical Properties of Carbonate Reservoirs, European Association of Geoscientists & Engineers 2020 (2020) 1–5. https://doi.org/10.3997/2214-4609.202010986.

[27] F. Amrouche, S.R. Gomari, M. Islam, X. Donglai, New Insights into the Application of a Magnetic Field to Enhance Oil Recovery from Oil-Wet Carbonate Reservoirs, Energy & Fuels 33 (2019) 10602–10610. https://doi.org/10.1021/acs.energyfuels.9b02296.

[28] F. Amrouche, S.R. Gomari, M. Islam, D. Xu, A novel hybrid technique to enhance oil production from oil-wet carbonate reservoirs by combining a magnetic field with alumina and iron oxide nanoparticles, J Clean Prod 281 (2021) 124891. https://doi.org/10.1016/j.jclepro.2020.124891.

[29] A. Instruments, Magnetic Field Calculator for Coils and Solenoids, (2022). https://www.accelinstruments.com/Magnetic/Magnetic-field-calculator.html.

[30] L. Chen, E. Bonaccurso, Electrowetting - From statics to dynamics, Adv Colloid Interface Sci 210 (2014) 2–12. https://doi.org/10.1016/j.cis.2013.09.007.

[31] M.S. Alnarabiji, M.M. Husein, Application of bare nanoparticle-based nanofluids in enhanced oil recovery, Fuel 267 (2020) 117262. https://doi.org/10.1016/j.fuel.2020.117262.

[32] A. Ali, H. Zafar, M. Zia, I. ul Haq, A.R. Phull, J.S. Ali, A. Hussain, Synthesis, characterization, applications, and challenges of iron oxide nanoparticles, Nanotechnol Sci Appl 9 (2016) 49–67. https://doi.org/10.2147/NSA.S99986.

[33] M.N. Agista, K. Guo, Z. Yu, A state-of-the-art review of nanoparticles application in petroleum with a focus on enhanced oil recovery, Applied Sciences (Switzerland) 8 (2018) 871. https://doi.org/10.3390/app8060871.

[34] P. Zhang, T. Austad, Wettability and oil recovery from carbonates: Effects of temperature and potential determining ions, Colloids Surf A Physicochem Eng Asp 279 (2006) 179–187. https://doi.org/10.1016/j.colsurfa.2006.01.009.

[35] M. Adil, H. Mohd Zaid, L. Kean Chuan, Electromagnetically-induced change in interfacial tension and contact angle of oil droplet using dielectric nanofluids, Fuel 259 (2020). https://doi.org/10.1016/j.fuel.2019.116274.

[36] H. Ali, H. Soleimani, N. Yahya, L. Khodapanah, M. Sabet, B.M.R. Demiral, T. Hussain, A.L. Lanre, Enhanced oil recovery by using electromagnetic-assisted nanofluids: A review, J Mol Liq (2020) 113095. https://doi.org/10.1016/j.molliq.2020.113095.

[37] S.H. Shafiai, A. Gohari, Conventional and electrical EOR review: the development trend of ultrasonic application in EOR, Journal of Petroleum Exploration and Production Technology 2020 10:7 10 (2020) 2923–2945. https://doi.org/10.1007/S13202-020-00929-X.

[38] M.M. Rehman, M. Meribout, Conventional versus electrical enhanced oil recovery: a review, J Pet Explor Prod Technol 2 (2012) 157–167. https://doi.org/10.1007/s13202-012-0034-x.

[39] M. Shalbafan, F. Esmaeilzadeh, G.R. Vakili-Nezhaad, Enhanced oil recovery by wettability alteration using iron oxide nanoparticles covered with PVP or SDS, Colloids Surf A Physicochem Eng Asp 607 (2020) 125509. https://doi.org/10.1016/j.colsurfa.2020.125509.

[40] G. Cheraghian, S. Rostami, M. Afrand, Nanotechnology in enhanced oil recovery, Processes 8 (2020) 1073. https://doi.org/10.3390/pr8091073.

[41] S. Vafaei, A. Purkayastha, A. Jain, G. Ramanath, T. Borca-Tasciuc, The effect of nanoparticles on the liquid-gas surface tension of Bi 2Te3 nanofluids, Nanotechnology 20 (2009) 185702. https://doi.org/10.1088/0957-4484/20/18/185702.

[42] C. Negin, S. Ali, Q. Xie, Application of nanotechnology for enhancing oil recovery – A review, Petroleum 2 (2016) 324–333. https://doi.org/10.1016/J.PETLM.2016.10.002.

[43] M.S. Kamal, A.A. Adewunmi, A.S. Sultan, M.F. Al-Hamad, U. Mehmood, Recent advances in nanoparticles enhanced oil recovery: Rheology, interfacial tension, oil recovery, and wettability alteration, J Nanomater 2017 (2017). https://doi.org/10.1155/2017/2473175.

[44] M. Adil, K. Lee, H.M. Zaid, N.R.A. Latiff, M.S. Alnarabiji, Experimental study on electromagnetic-assisted ZnO nanofluid flooding for enhanced oil recovery (EOR), PLoS One 13 (2018) e0193518. https://doi.org/10.1371/JOURNAL.PONE.0193518.

[45] B. Hascakir, C. Acar, S. Akin, Microwave-Assisted Heavy Oil Production: An Experimental Approach, Energy and Fuels 23 (2009) 6033–6039. https://doi.org/10.1021/EF9007517.

[46] K. Lee, M. Adil, H. Mohd. Zaid, B.H. Guan, H. Soleimani, M. Weis, Wettability, Interfacial Tension (IFT) and Viscosity Alteration of Nanofluids Under Electromagnetic (EM) Waves for Enhanced Oil Recovery (IFT) Applications, Advanced Structured Materials 92 (2019) 305–311. https://doi.org/10.1007/978-3-319-79005-3_21.

[47] A. Davletbaev, L. Kovaleva, T. Babadagli, Mathematical modeling and field application of heavy oil recovery by Radio-Frequency Electromagnetic stimulation, J Pet Sci Eng 78 (2011) 646–653. https://doi.org/10.1016/J.PETROL.2011.07.006.

[48] S. Al-Anssari, S. Wang, A. Barifcani, M. Lebedev, S. Iglauer, Effect of temperature and SiO2 nanoparticle size on wettability alteration of oil-wet calcite, Fuel 206 (2017) 34–42. https://doi.org/10.1016/j.fuel.2017.05.077.

[49] S. Al-Anssari, A. Barifcani, S. Wang, L. Maxim, S. Iglauer, Wettability alteration of oil-wet carbonate by silica nanofluid, J Colloid Interface Sci 461 (2016) 435–442. https://doi.org/10.1016/j.jcis.2015.09.051.

[50] M. Wang, L. Zhou, Y. Hou, W. He, W. Liu, F. Wu, X. Hou, Dynamic and reversible electrowetting with low voltage on the dimethicone infused carbon nanotube array in air, Chinese Chemical Letters 31 (2020) 1914–1918. https://doi.org/10.1016/J.CCLET.2020.04.059.

[51] Q.G. Xu, X.B. Liu, H.F. Zhang, Effect of direct electric current on wetting behavior of molten Bi on Cu substrate, Transactions of Nonferrous Metals Society of China 20 (2010) 1452–1457. https://doi.org/10.1016/S1003-6326(09)60320-4.

[52] F. Amrouche, D. Xu, New Approach to Assess the Impact of Wettability Alteration on rock compaction of carbonate reservoirs, in: First EAGE Rock Physics Workshop in Latin America, European Association of Geoscientists & Engineers, 2021: pp. 1–5. https://doi.org/10.3997/2214-4609.202187007.

[53] J.D. Sherwood, Breakup of fluid droplets in electric and magnetic fields, J Fluid Mech 188 (1988) 133–146. https://doi.org/10.1017/S0022112088000667.

[54] J. Jaraite, A. Kažukauskas, The profitability of electricity generating firms and policies promoting renewable energy, Energy Econ 40 (2013) 858–865. https://doi.org/10.1016/J.ENECO.2013.10.001.

[55] K.S. Hashim, A. Shaw, R. AlKhaddar, P. Kot, A. Al-Shamma'a, Water purification from metal ions in the presence of organic matter using electromagnetic radiation-assisted treatment, J Clean Prod 280 (2021) 124427. https://doi.org/10.1016/J.JCLEPRO.2020.124427.

685 [56] A. Al Helal, A. Soames, R. Gubner, S. Iglauer, A. Barifcani, Influence of magnetic fields on
686 calcium carbonate scaling in aqueous solutions at 150 °C and 1 bar, J Colloid Interface Sci 509
687 (2018) 472–484. https://doi.org/10.1016/J.JCIS.2017.09.028.

688 [57] A. Forgeron, Recovery of hydrocarbons using electrical stimulation, US20070102152A1, 2007.

689 [58] Y. Fu, P. Xie, P. Gu, J.J. Beaudoin, Effect of temperature on sulphate adsorption/desorption by
690 tricalcium silicate hydrates, Cem Concr Res 24 (1994) 1428–1432.
691 https://doi.org/10.1016/0008-8846(94)90156-2.

692

Declaration of interests

☒ The authors declare that they have no known competing financial interests or personal relationships that could have appeared to influence the work reported in this paper.

☐The authors declare the following financial interests/personal relationships which may be considered as potential competing interests: